Eur. Phys. J. Plus (2017) **132**: 173
DOI 10.1140/epjp/i2017-11416-x

THE EUROPEAN PHYSICAL JOURNAL PLUS

Regular Article

Electro-osmotic flow of couple stress fluids in a micro-channel propagated by peristalsis

Dharmendra Tripathi[1,a], Ashu Yadav[1], and O. Anwar Bég[2]

[1] Department of Mechanical Engineering, Manipal University Jaipur, Rajasthan - 303007, India
[2] Fluid Mechanics and Propulsion, Department of Mechanical and Aeronautical Engineering, Salford University, Newton Building, The Crescent, Salford, M54WT, England, UK

Received: 12 January 2017 / Revised: 19 February 2017
Published online: 14 April 2017 –

Abstract. A mathematical model is developed for electro-osmotic peristaltic pumping of a non-Newtonian liquid in a deformable micro-channel. Stokes' couple stress fluid model is employed to represent realistic working liquids. The Poisson-Boltzmann equation for electric potential distribution is implemented owing to the presence of an electrical double layer (EDL) in the micro-channel. Using long wavelength, lubrication theory and Debye-Huckel approximations, the linearized transformed dimensionless boundary value problem is solved analytically. The influence of electro-osmotic parameter (inversely proportional to Debye length), maximum electro-osmotic velocity (a function of external applied electrical field) and couple stress parameter on axial velocity, volumetric flow rate, pressure gradient, local wall shear stress and stream function distributions is evaluated in detail with the aid of graphs. The Newtonian fluid case is retrieved as a special case with vanishing couple stress effects. With increasing the couple stress parameter there is a significant increase in the axial pressure gradient whereas the core axial velocity is reduced. An increase in the electro-osmotic parameter both induces flow acceleration in the core region (around the channel centreline) and it also enhances the axial pressure gradient substantially. The study is relevant in the simulation of novel smart bio-inspired space pumps, chromatography and medical micro-scale devices.

1 Introduction

Electro-osmotic and electro-kinetic flows have stimulated significant interest for several decades, owing to advances in micro-fluidics technology. In such flows, the application of an external electric field mobilizes the bulk flow of electrolytes due to Coulombic forces exerted on ions present in the electric double layer. Developments in electro-osmotic pumping devices have been motivated not least due to new progress in astronautical systems, *e.g.*, heat pipes and alternative pumping systems for space stations [1–3]. They also find applications in medicine, industrial micro-flow control, actuators, mixing processes and chromotography [4–6]. The ever-growing sophistication of micro-fluidic devices requires enhanced levels of fluid control in micro-channels. The application of an electric field in micro-channels (on micro-electrodes) successfully generates electro-kinetic pumping. The most popular systems for electrically induced pumping exploit DC electro-osmotic phenomena and therefore need quite large voltages. Electro-osmotic pumping systems have the great advantage over other systems in that no moving parts are required which greatly reduces maintenance problems, especially for remote applications (space missions) [7,8]. These pumps can also achieve consistently high flow rates and pressures per device volume and are capable of functioning compactly with many different types of working fluid, *e.g.*, deionized water, acetone, buffered aqueous electrolytes, methanol, etc. In many of these systems, the operating fluid is non-Newtonian, *i.e.* it does not obey the Navier-Stokes viscous flow model. Working fluids may be doped with suspensions, additives and other agents. These result in shear-stress strain characteristics which deviate from the Newtonian model. Although many models have been developed for simulating the rheological behaviour of fluids in electro-osmotic micro-devices, the couple stress model offers characteristics which cannot be captured with other models (viscoplastic, viscoelastic, shear-thinning, etc.). The presence of the micro-structures in many fluids employed in electrokinetics suggests that the particle-size effect is significant and this is best described with a micro-structural or micro-continuum model of which couple stress fluids are a simple case. Introduced by Stokes [9] to

[a] e-mail: dharmtri@gmail.com (corresponding author)

mimic particle-size effects, Stokes' micro-continuum theory is a generalization of the classical theory of fluids where polar effects, such as the presence of couple stresses, body couples, and an anti-symmetric stress tensor are taken into consideration. It is therefore a more realistic constitutive model in which the couple stress effects are considered as a consequence of the action of a deforming body on its neighbourhood. Couple stresses have been identified in real working fluids which have large molecules. Couple stress theory has been implemented in many branches of engineering, biology and energy systems including lubrication design [10,11], hemodynamic filtration systems [12], blood flows [13] and magnetohydrodynamics [14]. Using appropriate mathematical models and numerical/analytical methods, the dynamics of couple stress fluids can be simulated quite accurately as demonstrated in [10–14].

Peristaltic pumping is a significant biological mechanism which is generated by the symmetrical contraction and expansion of a flexible boundary. It arises in many diverse systems in human physiology and nature including embryological transport, earthworm and snake locomotion, plant trans-location (phloem dynamics) and gastro-intestinal motion. A comprehensive analysis of peristaltic flow has been made by Fung [15]. Other fundamental studies of peristaltic propulsion have been conducted by Jaffrin and Shapiro [16], and Brown and Hung [17]. In the context of biomimetic pumping systems for spacecraft systems, important progress was made at Caltech's Jet Propulsion Laboratory (JPL) in the 1990s, as elaborated by Bar-Cohen and Chatig [18]. These bio-inspired peristaltic pumps for chemical and nuclear engineering waste transport have been shown to avoid the inherent problems of conventional pumping systems, *e.g.*, leakage, backflow, corrosion, bubble formation, etc. Further details are documented in Shkolnikov *et al.* [19]. Stimulated by these and other applications, mathematical modelling of peristaltic flows of couple stress fluids has also received extensive attention. Elsehawey and Mekheimer [20] presented perturbation solutions for peristaltic pumping generated via a sinusoidal travelling wave along the walls of a two-dimensional channel filled with a viscous incompressible couple-stress fluid, observing that with an increase in couple stress parameter the mean axial flow is strongly decelerated. Mekheimer and Abdelmaboud [21] investigated theoretically the influence of an endoscope on the peristaltic flow of a couple stress fluid in an annulus under lubrication approximations, showing that pressure rise, frictional forces and trapping phenomena are all modified substantially with couple stresses. Other studies of peristaltic propulsion of couple stress fluids include Rathod *et al.* [22] who employed Beavers-Joseph boundary conditions and Ramesh and Devakar [23] who considered magnetohydrodynamic heat and mass transfer effects. Abdelmaboud *et al.* [24] derived analytical solutions for axial velocity, stream function, temperature and axial pressure gradient in two-dimensional thermo-fluid peristaltic pumping of couple stress fluids. Tripathi and Bég [25] presented closed-form solutions for magnetized unsteady peristaltic propulsion of electrically conducting, couple stress fluids in a finite length channel, noting that increasing couple stress effect induces axial flow acceleration and pressure gradient reduction.

The above studies did not simultaneously consider electro-osmotic transport in non-Newtonian fluids. In recent years this area has become increasingly attractive to researchers owing to newly fabricated electro-rheological fluids which can combine desirable electro-kinetic and non-Newtonian effects in micro-scale devices. Several theoretical investigations have therefore been reported using a variety of robust non-Newtonian formulations. Li *et al.* [26] derived closed-form solutions for the electrical potential distribution in rotating electro-osmotic flow of an incompressible third grade Reiner-Rivlin fluids in a micro-channel, observing that with increasing dimensionless electro-kinetic width, increasing Reynolds number and non-Newtonian parameter, the flow is decelerated and volumetric flow rates reduced. Siddiqui and Lakhtakia [27] investigated transient electro-osmotic flow of an Eringen micro-polar fluid in a rectangular micro-channel with height significantly greater than the Debye length, noting that under a spatially uniform electric field (applied as an impulse of finite magnitude), decay times of the fluid velocity are markedly lesser for micro-polar fluids than Newtonian fluids. Afonso *et al.* [28] used the Phan-Thien–Tanner (PTT) constitutive equation to simulate electro-osmotic viscoelastic flow in a channel with pressure gradient and asymmetric boundary conditions (different zeta potentials at the walls). Sousa *et al.* [29] further studied electro-osmosis and pressure gradient forcing in PTT viscoelastic micro-channel Poiseuille skimming flows. Tang *et al.* [30] used a lattice Boltzmann method to computationally simulate the electroosmotic power-law rheological flow in micro-channels, showing that power-law index markedly alters the electroosmotic flow pattern and that shear thinning fluids constrain the electrical double layer effect in a small zone nearer the wall surface. Tang *et al.* [31] used the Herschel-Bulkley model to analyse viscoplastic pressure-driven electro-osmotic flow of non-Newtonian fluids in porous media. Li *et al.* [32] studied analytically time-dependent electroosmotic flow of generalized Maxwell viscoelastic fluids through both a micro-parallel channel and a micro-tube, deriving close-form solutions for the linearized Poisson-Boltzmann equation. Rezaei *et al.* [33] investigated the effect of electric field and temperature on electrokinetic flow characteristics. Shit *et al.* [34] presented a mathematical model to analyze the electroosmotic flow of power-law fluids through a micro-channel and discussed the effects of Joule heating and thermal radiation. In another investigation [35], they have studied electro-osmosis modulated MHD flow and heat transfer through the micro-channel. They have observed that magnetic field and Joule heating are significantly responsible for electroosmotic flow control.

These investigations did not consider electro-osmotic peristaltic flows, *i.e.* they assumed the channel boundaries to be rigid. However both Newtonian and non-Newtonian electro-osmotic peristaltic flows have been addressed owing to their significance in novel micro-fluid devices. El Sayed *et al.* [36] used the Oldroyd viscoelastic model to analyze dielectric peristaltic pumping in a channel with heat transfer effects. Goswami *et al.* [37] used the Ostwald-DeWaele

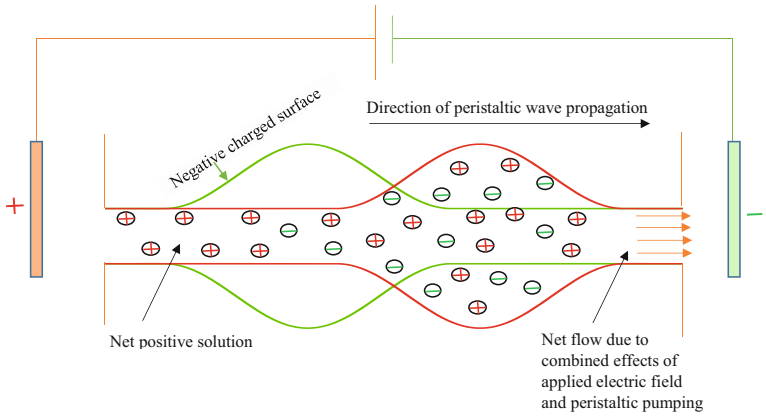

Fig. 1. Schematic of the peristaltic transport of an aqueous electrolyte couple stress fluid through a flexible parallel plate micro-channel.

model to analyze both shear thinning and thickening electro-kinetic peristaltic pumping. Further studied include Chakraborty [38] and Tripathi *et al.* [39]. Electrofluid dynamics of couple stress fluids has also found interest among smart materials systems. Excellent studies in this regard include the works of Rudraiah *et al.* [40], Shankar *et al.* [41] and Rudraiah *et al.* [42] which have explored electrical Rayleigh number effects, interphase mass transfer and travelling-wave mode hydrodynamic stability aspects. Further investigations on peristaltic transport of nanofluids through asymmetric channels have considered Williamson fluid flow through stenosed arteries, water/ethylene glycol based nanofluids and Jeffrey fluids in a non-uniform rectangular duct [43–47].

In the present article, we consider for the first time, the peristaltic transport of an aqueous electrolyte solution (simulated as a couple stress non-Newtonian suspension) through a flexible micro-channel. Analytical solutions for the linearized transformed dimensionless boundary value problem are derived for axial velocity, volumetric flow rate, pressure gradient, local wall shear stress and stream function. The influence of electro-osmotic (EO) parameter, κ (inversely proportional to the Debye length ($\kappa = aez\sqrt{\frac{2n_0}{\varepsilon K_B T}} = \frac{a}{\lambda_d}$)), maximum electro-osmotic velocity (U_{HS}, which is directly proportional to external applied electrical field, E_ξ, since $U_{HS} = -\frac{E_\xi \varepsilon \zeta}{\mu c}$), and couple stress parameter (α) on the flow characteristics is evaluated in detail. Trapping phenomena are also examined. The work is relevant to smart EO space pumps and medical micro-fluidics.

2 Mathematical formulation and analytical solution

Peristaltic transport of an aqueous electrolyte couple stress non-Newtonian fluid solution through a flexible walled two-dimensional micro-channel is considered, as depicted in fig. 1. Couple stress fluids are a sub-set of *polar non-Newtonian fluid theories*, which considers couple stresses in addition to the classical Cauchy stresses in viscous fluid dynamics. Unlike other more complex micro-continuum models, the kinematics of such fluids is completely encompassed in the *velocity field*, as elaborated by Eringen [48]. The concept of couple stresses arises from the consideration of mechanical interactions in the fluid medium. The key characteristic of couple stresses is to introduce a *length-dependent effect*, which is absent in the classical non-polar fluid dynamics (Navier-Stokes) model. The advantage of the couple stress model is that although it introduces extra terms, which are of fourth order (maximum case), these terms are *linear*. It is therefore much simpler than other nonlinear micro-stuctural non-Newtonian models, yet representative of the physics of many important thermal process fluids. The main effect of couple stresses is to introduce a *size-dependent effect* that is not present in the classical viscous theories. In the latter the *stress tensor* is symmetric as a result of assuming there is no rotational interaction among particles. However, this cannot be true for the cases of fluid flow with suspended particles (of interest in electro-kinetic propulsion) and thus the need of couple stress theory arises. In fact the micro-rotation of freely suspended particles gives rise to an *anti-symmetric stress*, known as couple stress. The need for a separate spin momentum (micro-rotation) balance is therefore not required, as with micro-polar fluids. Implicit in the present simulations is the assumption of zero angular velocity at the micro-channel walls, *i.e.* vanishing of couple stresses and hence zero traction due to couple stresses must also be zero there as noted by Naduvinamani and Siddangouda [49]. The geometry of the flexible channel walls is defined analytically as follows:

$$h(x,t) = a - b\cos^2\frac{\pi}{\lambda}(x - ct), \tag{1}$$

where a, b, λ, x, c, and t are the half width at the inlet, amplitude, wavelength, axial coordinate, wave velocity, and time, respectively. In fig. 1, a peristaltic wave propagates from the left reservoir (Anode, +ve ion) to the right reservoir (Cathode, −ve ion) with a wave velocity c.

The equations of motion that characterize a couple stress fluid flow under the effect of an axial external electric field are given, in vector form, by (refs. [10–14])

$$\frac{\mathrm{d}\rho}{\mathrm{d}t} + \rho\,\mathrm{div}(\vec{q}) = 0, \tag{2}$$

$$\rho\frac{\mathrm{d}\vec{q}}{\mathrm{d}t} = \rho\vec{f} + \frac{1}{2}\,\mathrm{curl}(\rho\vec{C}) + \mathrm{div}(\vec{\tau}^{(s)}) + \frac{1}{2}\,\mathrm{curl}(\mathrm{div}(\vec{M})) + \rho_e E_x, \tag{3}$$

where ρ is the density of the fluid, $\vec{q}$ is velocity vector, $\vec{\tau}^{(s)}$ is the symmetric part of the force stress diad, $\vec{M}$ is the couple stress diad and $\vec{f}$, $\vec{C}$ are the body force per unit mass and body couple per unit mass, respectively, and E_x represents the axial applied electric field. The constitutive equations concerning the force stress t_{ij} and the rate of deformation tensor d_{ij} are given by (refs. [10–14])

$$t_{ij} = -p\delta_{ij} + \lambda\,\mathrm{div}(\vec{q})\delta_{ij} + 2\mu d_{ij} - \frac{1}{2}\varsigma_{ijk}\big[m_{,k} + 4\eta w_{k,rr} + \rho\vec{C}_k\big]. \tag{4}$$

The couple stress tensor m_{ij} that arises in the theory has the linear constitutive relation [10–14]

$$m_{ij} = \frac{1}{3}m\delta_{ij} + 4\eta w_{j,i} + 4\eta' w_{i,j}, \tag{5}$$

where $w = \frac{1}{2}\,\mathrm{curl}(\vec{q})$ is the spin vector, $w_{i,j}$ is the spin tensor, m is the trace of couple stress tensor m_{ij}, p is the fluid pressure and $\rho\vec{C}_k$ is the body couple vector. A comma in the suffixes denotes covariant differentiation and $w_{k,rr}$ stands for $w_{k,11} + w_{k,22} + w_{k,33}$. The quantities λ and μ are the viscosity coefficients and η, η' are the couple stress viscosity coefficients. These material constants are constrained by the inequalities

$$\mu \geq 0; \qquad 3\lambda + 2\mu \geq 0; \qquad \eta \geq 0; \qquad |\eta'| \leq \eta. \tag{6}$$

If the fluid is incompressible, in the absence of body forces and body couples the above field equations (2) and (3) reduce to

$$\mathrm{div}(\vec{q}) = 0, \tag{7}$$

$$\rho\left[\frac{\partial\vec{q}}{\partial t} + (\vec{q}\cdot\nabla\vec{q})\right] = -\mathrm{grad}(p) - \mu\,\mathrm{curl}(\mathrm{curl}(\vec{q})) - \eta\,\mathrm{curl}(\mathrm{curl}(\mathrm{curl}(\mathrm{curl}(\vec{q})))) + \rho_e E_x. \tag{8}$$

The Poisson-Boltzmann equation for electric potential distribution is employed due to the presence of EDL in the micro-channel and is defined as

$$\nabla^2\Phi = -\frac{\rho_e}{\varepsilon}\,. \tag{9}$$

Here ∇^2 is the two-dimensional Laplacian operator, ρ_e is the density of the total ionic change and ε is the permittivity. For a symmetric $(z:z)$ electrolyte, the density of the total ionic energy, ρ_e is given by

$$\rho_e = ez(n^+ - n^-). \tag{10}$$

Here n^+ and n^- are the number of densities of cations and anions, respectively, and are given by the Boltzmann distribution (considering no EDL overlap) which takes the form

$$n^{\pm} = n_0\mathrm{Exp}\left[\pm\frac{ez\Phi}{K_B T}\right]. \tag{11}$$

In eq. (11), n_0 represents the concentration of ions at the bulk, which is independent of surface electro-chemistry, e is the electronic charge, z is the charge balance, K_B is the Boltzmann constant, T is the average temperature of the electrolytic solution. Introducing a normalized electro-osmotic potential function Φ with zeta potential ζ of the medium along with other non-dimensional variables, like $\bar{\Phi} = \frac{\Phi}{\zeta}$, we invoke the Debye-Huckel linearization approximation, namely,

$$\sinh\left(\frac{ez\Phi}{K_B T}\right) \approx \frac{ez\Phi}{K_B T}\,. \tag{12}$$

Furthermore imposing the boundary conditions $\frac{\partial \Phi}{\partial y}|_{y=0} = 0$ and $\Phi|_{\eta=y} = 1$, the *potential function* is obtained as

$$\Phi = \frac{\cosh(\kappa y)}{\cosh(\kappa h)}\,. \tag{13}$$

Here $\kappa = aez\sqrt{\frac{2n_0}{\varepsilon K_B T}} = \frac{a}{\lambda_d}$ is known as the *electro-osmotic parameter* and $\lambda_d \propto \frac{1}{\kappa}$ is the *Debye length* or characteristic thickness of the electrical double layer (EDL). To facilitate analytical solutions, it is advantageous to introduce a group of non-dimensional parameters to transform the boundary value problem. Noting that the nonlinear terms in the momentum equation (8) are $O(Re\,k^2)$, proceeding with the analysis, we define

$$\bar{x} = \frac{x}{\lambda}\,, \quad \bar{y} = \frac{y}{a}\,, \quad \bar{t} = \frac{tc}{\lambda}\,, \quad \bar{u} = \frac{u}{c}\,, \quad \bar{v} = \frac{v}{kc}\,, \quad \bar{p} = \frac{pa^2}{\mu c \lambda}\,. \tag{14}$$

Here $Re = \frac{c\lambda}{\mu/\rho}$ is the Reynolds number (based on peristaltic wavelength and velocity), $k = \frac{a}{\lambda}$ denotes the ratio of the transverse length scale to the axial length scale, and $l = \frac{1}{\alpha} = \frac{1}{a}\sqrt{\frac{\eta}{\mu}}$ is the length parameter, which is a characteristic measure of the "polarity" of the fluid model, and this parameter is identically zero in the case of non-polar fluids (vanishing couple stresses). Therefore, the nonlinear terms may be dropped in the limit that $Re,\, k \to 1$. In this limit, governing equations are reduced to the linearized system:

$$\frac{\partial u}{\partial x} + \frac{\partial v}{\partial y} = 0, \tag{15}$$

$$\frac{\partial p}{\partial x} = \frac{\partial^2 u}{\partial y^2} - \frac{1}{\alpha^2}\frac{\partial^4 u}{\partial y^4} - +\kappa^2 U_{HS}\Phi. \tag{16}$$

Imposing the following boundary conditions:

$$u|_{y=h} = 0, \qquad \left.\frac{\partial u}{\partial y}\right|_{y=0} = 0, \qquad \left.\frac{\partial^2 u}{\partial y^2}\right|_{y=h} = 0, \qquad \left.\frac{\partial^3 u}{\partial y^3}\right|_{y=0} = 0, \tag{17}$$

solving the linearized axial momentum equation (16) by virtue of the boundary conditions (17), the *axial velocity* emerges as

$$\begin{aligned} u = \frac{e^{-y\alpha}}{2\alpha^2(1+e^{2h\alpha})(\alpha^2-\kappa^2)}\Bigg\{ & (2e^{h\alpha} + 2e^{(h+2y)\alpha})\left(-\alpha^2\frac{\partial p}{\partial x} + \kappa^2\left(\frac{\partial p}{\partial x} + \alpha^2 U_{HS}\right)\right) \\ & + (2e^{y\alpha} + 2e^{(h+2y)\alpha})(\alpha^2-\kappa^2)\left(2\alpha^2 U_{HS} + \frac{\partial p}{\partial x}(2 - \alpha^2 h^2 + \alpha^2 y^2)\right) - 2\alpha^4 U_{HS}\, e^{y\alpha}(1+e^{2h\alpha})\cosh(\kappa y)\cosh(\kappa h)\Bigg\}. \end{aligned} \tag{18}$$

The *volumetric flow rate* is computed by integrating axial velocity across the channel width and is found to be

$$Q = \int_0^h u\mathrm{d}y. \tag{19}$$

Using eq. (18) in eq. (19), we arrive at

$$Q = \frac{\left\{\begin{array}{l} \kappa\left(3\alpha^5 h U_{HS}(1+e^{2h\alpha}) - \alpha^2\frac{\partial p}{\partial x}(-3 - 3\alpha h + \alpha^3 h^3 + e^{2h\alpha}(3 - 3\alpha h + \alpha^3 h^3))\right) \\ +\kappa^2\left(-3\alpha^2 U_{HS}(1 + \alpha h + e^{2h\alpha}(-1+\alpha h)) + \frac{\partial p}{\partial x}(-3 - 3\alpha h + \alpha^3 h^3 + e^{2h\alpha}(3 - 3\alpha h + \alpha^3 h^3))\right) \\ -3\alpha^5 U_{HS}\tanh(\kappa h)(1+e^{2h\alpha}) \end{array}\right\}}{3\kappa\alpha^3(\alpha^2-\kappa^2)(1+e^{2h\alpha})}\,. \tag{20}$$

Rearranging the terms of eq. (20), the *axial pressure gradient* is obtained as

$$\frac{\partial p}{\partial x} = \frac{\left\{\begin{array}{l} 3\alpha^2(\kappa(\alpha^3(1+e^{2h\alpha})(Q - hU_{HS}) + \kappa^2(-Q\alpha(1+e^{2h\alpha}) \\ +U_{HS}(1 + h\alpha + e^{2h\alpha}(-1+h\alpha)))) + \alpha^3 U_{HS}\tanh(\kappa h)(1+e^{2h\alpha}))) \end{array}\right\}}{\kappa(\kappa^2-\alpha^2)(-3 - 3h\alpha + h^3\alpha^3 + e^{2h\alpha}(3 - 3h\alpha + h^3\alpha^3))}\,. \tag{21}$$

The pressure difference across one wavelength is defined as

$$\Delta p = \int_0^1 \frac{\partial p}{\partial x} \mathrm{d}x. \tag{22}$$

The *local wall shear stress*, defined as $\tau_w = \frac{\partial u}{\partial y}|_{y=h}$, may then also be computed based on eq. (18)

$$\tau_w = \frac{\left\{ \begin{array}{l} \frac{\partial p}{\partial x}\alpha^2(1+h\alpha+e^{2h\alpha}(-1+h\alpha)) - \kappa^2(\alpha^2 U_{HS}(1-e^{2h\alpha}) \\ +\frac{\partial p}{\partial x}(1+h\alpha+e^{2h\alpha}(-1+h\alpha))) - \kappa\alpha^3 U_{HS}\tanh(\kappa h)(1+e^{2h\alpha}) \end{array} \right\}}{\alpha(1+e^{2h\alpha})(\alpha^2-\kappa^2)}. \tag{23}$$

The transformations between a wave frame (x_w, y_w) moving with velocity c and the fixed frame (x, y) are given by

$$x = x_w - ct, \qquad y = y_w, \qquad u = u_w + c, \qquad v = v_w, \tag{24}$$

where (u_w, v_w) and (u, v) are the velocity components in the wave and fixed frame, respectively.

The volumetric flow rate in the wave frame is given by

$$q_w = \int_0^h u_w \mathrm{d}y_w = \int_0^h (u-1)\mathrm{d}y_w, \tag{25}$$

which, on integration, yields

$$q_w = Q - h. \tag{26}$$

Averaging the volumetric flow rate along one time period, we get

$$\bar{Q} = \int_0^1 Q\mathrm{d}t = \int_0^1 (q_w + h)\mathrm{d}t, \tag{27}$$

which, on integration, yields

$$\bar{Q} = q_w + 1 - \phi/2 = Q + 1 - h - \phi/2. \tag{28}$$

Using the D'Alembert mass conservation equation (15), the stream function (obeying the Cauchy-Riemann equations, $u = \frac{\partial \psi}{\partial y}$ and $v = -\frac{\partial \psi}{\partial x}$) is also readily derived as

$$\begin{aligned} \psi = &-\Big(e^{-y\alpha}\left(\cosh(\kappa h)+\sinh(\kappa h)\right)\Big(\kappa(e^{(h+2y)\alpha}\left(-6(Q-hU_{HS})\alpha^2+\kappa^2(6Q-2h^3U_{HS}\alpha^2)\right) \\ &+2e^{h\alpha}\left(3(Q-hU_{HS})\alpha^2+\kappa^2(-3Q+h^3U_{HS}\alpha^2)\right)+e^{(2h+y)\alpha}y\alpha(-\kappa^2(U_{HS}\alpha(-3h^2+y^2+h^3\alpha-hy^2\alpha) \\ &+Q(-6+3h^2\alpha^2-y^2\alpha^2))+\alpha(Q\alpha(6-3h^2\alpha^2+y^2\alpha^2)+U_{HS}(-6+h^3\alpha^3-hy^2\alpha^3))) \\ &+e^{y\alpha}y\alpha(\kappa^2(U_{HS}\alpha(-3h^2+y^2-h^3\alpha+hy^2\alpha)+Q(-6+3h^2\alpha^2-y^2\alpha^2))+\alpha(Q\alpha(6-3h^2\alpha^2+y^2\alpha^2) \\ &+U_{HS}(6+h^3\alpha^3-hy^2\alpha^3))))\cosh(\kappa h)+U_{HS}\alpha^2((6e^{h\alpha}-6e^{(h+2y)\alpha}+e^{y\alpha}y\alpha(6-3h^2\alpha^2+y^2\alpha^2) \\ &+e^{(2h+y)\alpha}y\alpha(6-3h^2\alpha^2+y^2\alpha^2))\sinh(\kappa h)+2e^{y\alpha}(-3-3h\alpha+h^3\alpha^3+e^{2h\alpha}(3-3h\alpha+h^3\alpha^3))\sinh(\kappa y))\Big) \\ &\times(1-\tanh(\kappa h))\Big)\Big/2\kappa(-\kappa^2+\alpha^2)(-3-3h\alpha+h^3\alpha^3+e^{2h\alpha}(3-3h\alpha+h^3\alpha^3)). \end{aligned} \tag{29}$$

3 Numerical results and discussion

Extensive computations have been performed using the Mathematica symbolic software and are presented in figs. 2(a)–(c), 3(a)–(c), 4(a)–(c), 5(a)–(c) and 6(a)–(g).

Figures 2(a)–(c) illustrate the evolution in axial velocity across the channel span with variation in electro-osmotic parameter (κ), maximum electro-osmotic velocity (U_{HS}) and non-Newtonian couple stress parameter (α), respectively. With increasing κ values, fig. 2(a) shows that, under constant axial pressure gradient ($\frac{\partial p}{\partial x} = 1$) there is a strong acceleration in axial velocity in the vicinity of the micro-channel walls and a very weak acceleration in the core zone (around the centre line). In the central zone there is however a symmetric drop in axial velocity and a weak increase at the centre line, irrespective of the value of electro-osmotic parameter. This parameter arises in the electrical potential term in the linearized momentum eq. (16), $\kappa^2 U_{HS}\Phi$. We note that in the limiting case of $\kappa \to \infty$ the axial velocity (9)

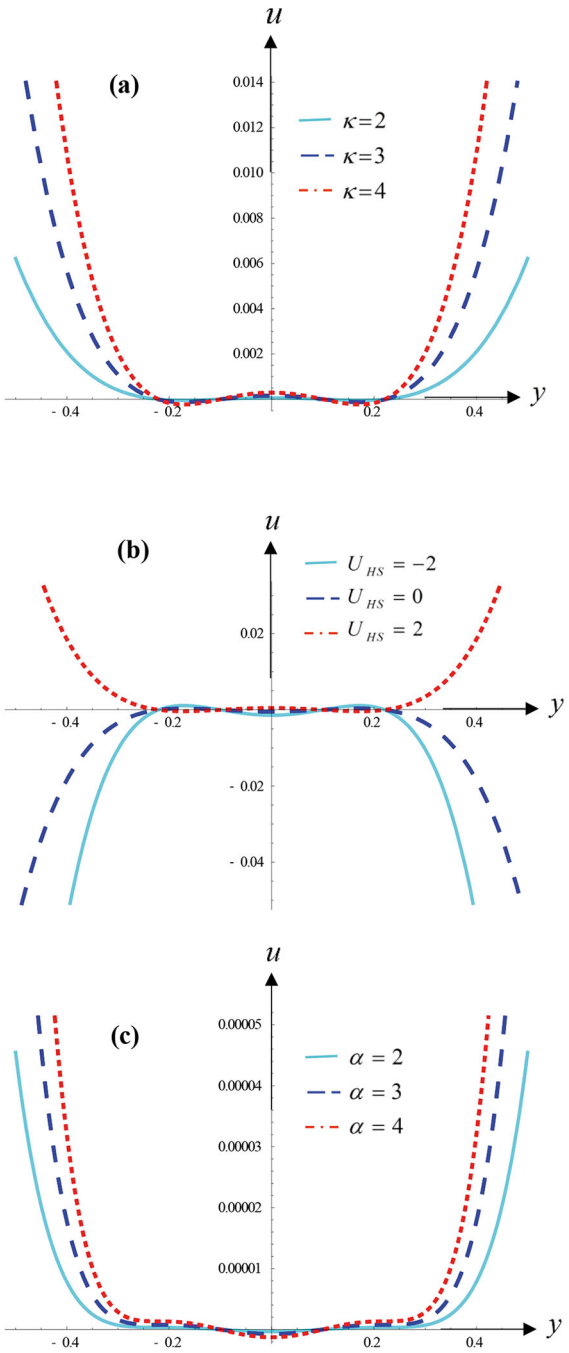

Fig. 2. Velocity profile (axial velocity *vs.* transverse coordinate) at $\phi = 0.9$, $x = 1.0$, $\frac{\partial p}{\partial x} = 1$ and (a) $U_{HS} = 1$, $\alpha = 1$ (b) $\kappa = 1$, $\alpha = 5$ (c) $U_{HS} = 1$, $\kappa = 1$.

reduces to the case for *electro-kinetic couple stress peristaltic transport through a very thin electric double layer*. Evidently the electro-kinetic body force effect aids momentum development in the micro-channel and achieves a non-trivial acceleration effect. Furthermore with the additional condition of $\alpha \to 0$, we obtain the *electro-kinetic Newtonian peristaltic transport through a very thin electric double layer*. Figure 2(b) demonstrates that, for negative or zero values of the maximum electro-osmotic velocity, *i.e.* Helmholtz-Smoluchowski velocity (U_{HS}), axial velocity magnitudes are consistently negative across the channel span. However for $U_{HS} > 0$ the profiles are positive and reflective symmetry is observed about the y-axis. Increasing electro-osmotic velocity clearly induces a substantial acceleration in the axial flow. Figure 2(c) shows that with increasing couple stress parameter (decreasing couple stress effect), the axial flow is accelerated in proximity to the micro-channel walls and also in zones on either side of the channel centre line. However at the centre line, *i.e.* the centre of the core flow zone, there is a slight deceleration generated with greater couple stress effect. The couple stress parameter arises as an inverse function in the linear fourth order derivative,

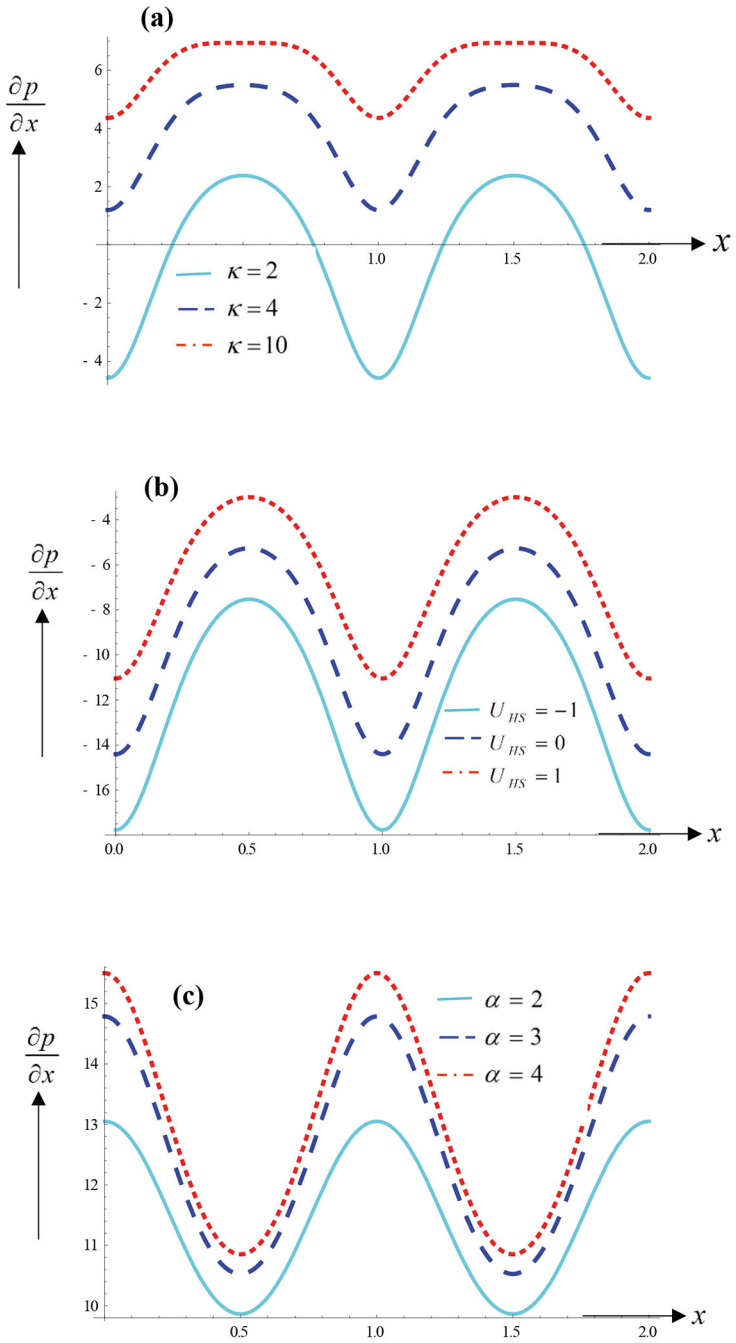

Fig. 3. Pressure gradient along the channel length at $\phi = 0.2$, $Q = 0.5$ and (a) $U_{HS} = 5$, $\alpha = 1$ (b) $\kappa = 5$, $\alpha = 1$ (c) $U_{HS} = 5$, $\kappa = 10$.

$-\frac{1}{\alpha^2}\frac{\partial^4 u}{\partial y^4}$. As α values increase the contribution of this body force is reduced and this implies that stronger polarity, *i.e.* greater couple stress effect the flow will be decelerated, an observation which concurs with many other studies including the non-electrical peristaltic flow analysis of Elsehawey and Mekheimer [26] and the electrical couple stress model of Shankar *et al.* [44]. Furthermore this observation has also been confirmed in the seminal work of Cowin [50].

Figures 3(a)–(c) illustrate the distributions of axial pressure gradient ($\frac{\partial p}{\partial x}$) with axial coordinate (x) with different values of the electro-osmotic parameter (κ), maximum electro-osmotic velocity (U_{HS}) and non-Newtonian couple stress parameter (α), respectively. The periodic nature of the flow is clearly captured in these visualizations and is caused by the peristaltic wave motion, *i.e.* successive troughs and peaks in pressure gradient. Increasing electro-osmotic parameter (κ) markedly elevates the magnitudes of pressure gradients and eliminates the negative values observed for lower κ values. The sharper profiles computed with lower electro-osmotic parameter are also smoothed somewhat to more oblate, flattened distributions with greater electro-osmotic effect, *i.e.* higher κ values. Figure 3(b) shows that with

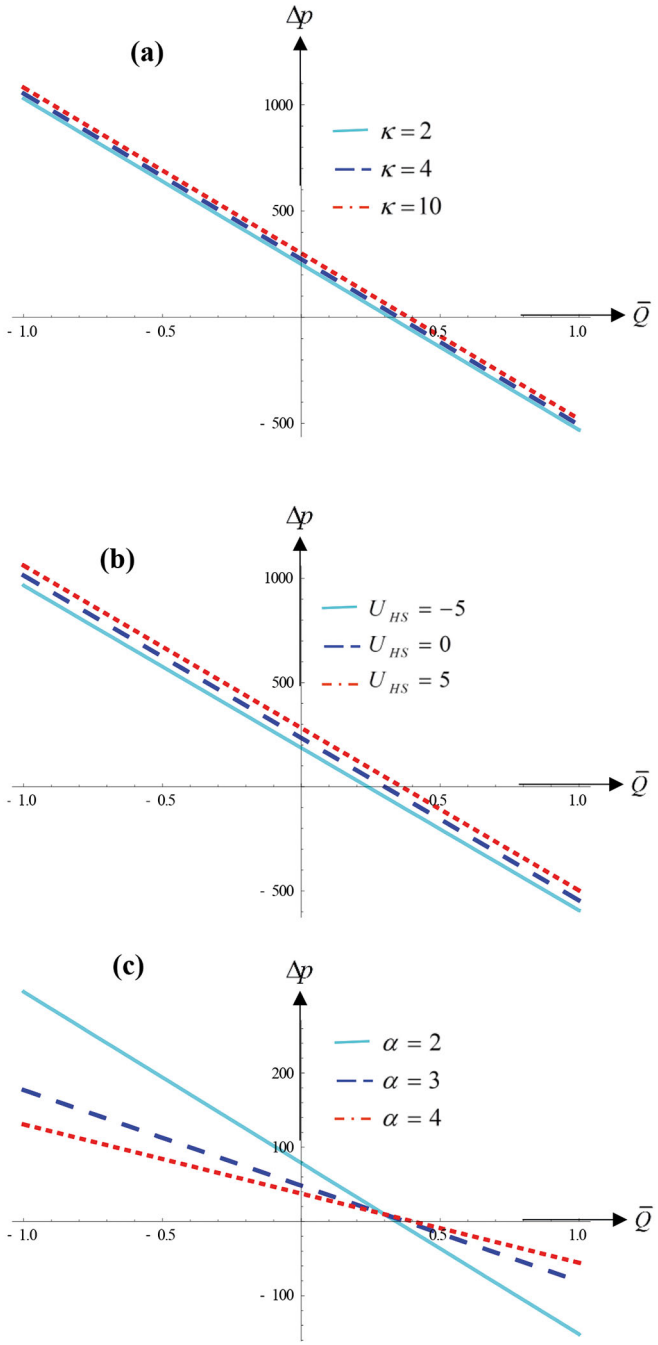

Fig. 4. Pressure difference across one wavelength *vs.* time averaged volumetric flow rate at $\phi = 0.2$, $Q = 0.5$ and (a) $U_{HS} = 5$, $\alpha = 1$ (b) $\kappa = 5$, $\alpha = 1$ (c) $U_{HS} = 1$, $\kappa = 5$.

increasing Helmholtz-Smoluchowski velocity (U_{HS}) from negative, through zero, to positive values, a *significant reduction* in pressure gradient magnitudes is generated along the entire x-axis. On the other hand, a strong enhancement in pressure gradient is also computed with increasing couple stress parameter, α, *i.e.* weaker couple stress body force effect in fig. 3(c). The influence of all the key electro-physical and rheological parameters is significant and demonstrates that even for linearized models, as elaborated in the present work, these effects can still retain an important influence.

Figures 4(a)–(c) illustrate the evolution in pressure difference across one wavelength *vs.* time averaged volumetric flow rate for different values of the electro-osmotic parameter (κ), maximum electro-osmotic velocity (U_{HS}) and non-Newtonian couple stress parameter (α), respectively. These graphs provide a perspective of the response in pressure difference for both positive (aligned in the direction of axial electrical field) and negative (opposite to axial field orientation, *i.e.* x-axis) to a change in time-averaged volumetric flow rate ($\bar{Q}$). Maximum flow rate, Q is however fixed at 0.5 and the peristaltic wave amplitude is relatively low at $\phi = 0.2$ in these plots. With an increase in electro-osmotic

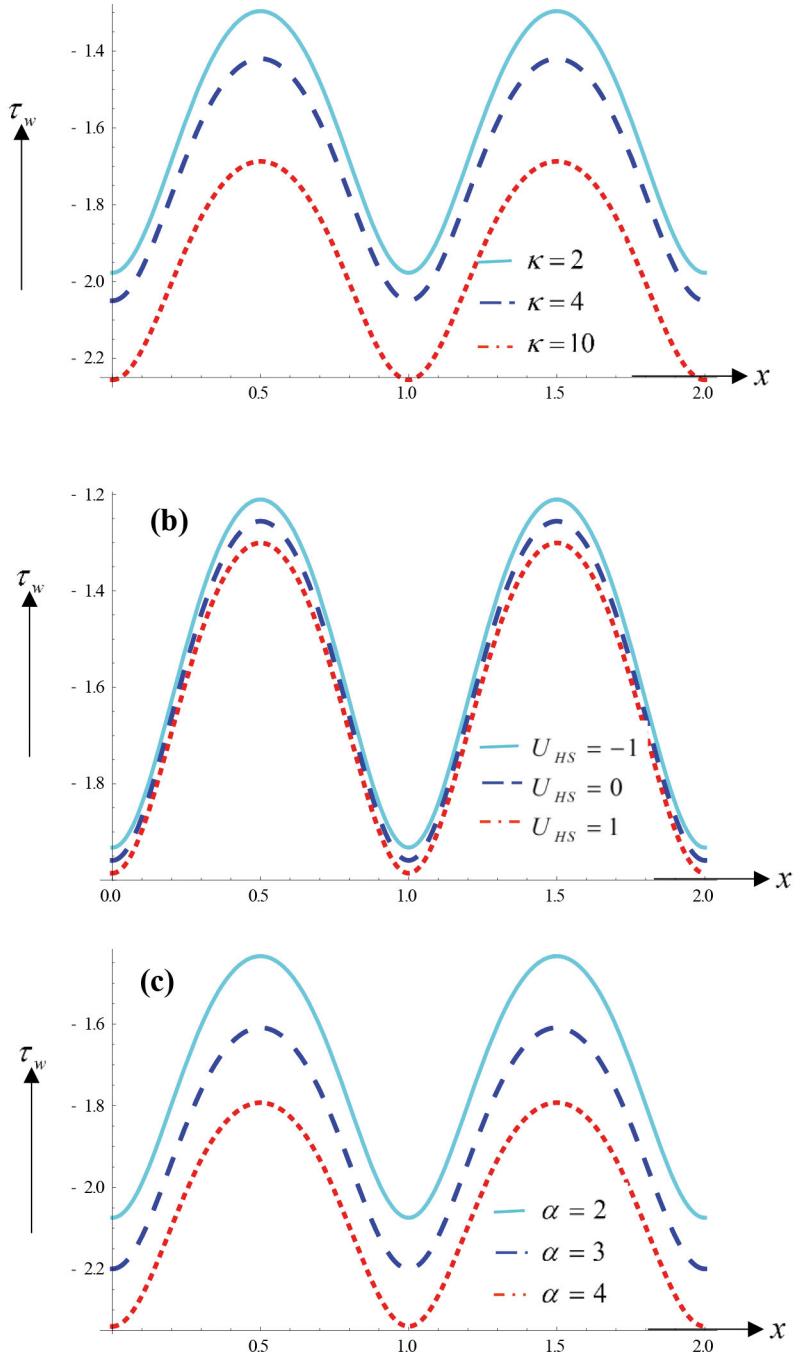

Fig. 5. Local wall shear stress along the channel at $\phi = 0.2$, $Q = 0.5$ and (a) $U_{HS} = 5$, $\alpha = 1$ (b) $\kappa = 5$, $\alpha = 1$ (c) $U_{HS} = 1$, $\kappa = 5$.

parameter, as depicted in fig. 4(a), there is a *consistent albeit weak* enhancement in pressure difference for both $\bar{Q} < 0$ and $\bar{Q} > 0$. However negative pressure difference is always associated with negative flow rate and vice versa for positive flow rate. Pressure difference never vanishes for any value of Q. Clearly the electro-osmotic effect exerts a tangible influence on pressure difference in the peristaltic regime. Similarly, fig. 4(b) reveals that with increasing Helmholtz-Smoluchowski velocity, *i.e.* greater strength of imposed axial electrical field, there is also an associated increase in pressure difference, again for both negative and positive flow rates. The influence is again sustained irrespective of values of $\bar{Q}$. Again vanishing pressure difference is never computed at any value of flow rate. Greater axial electrical field therefore generally boosts the pressure difference in the regime and this will contribute to an increase in efficiency of peristaltic propulsion in the systems. It causes a stronger influence than the electro-osmotic effect. Figure 4(c) shows that couple stress parameter (and therefore couple stress effect) induces less consistent modification in pressure

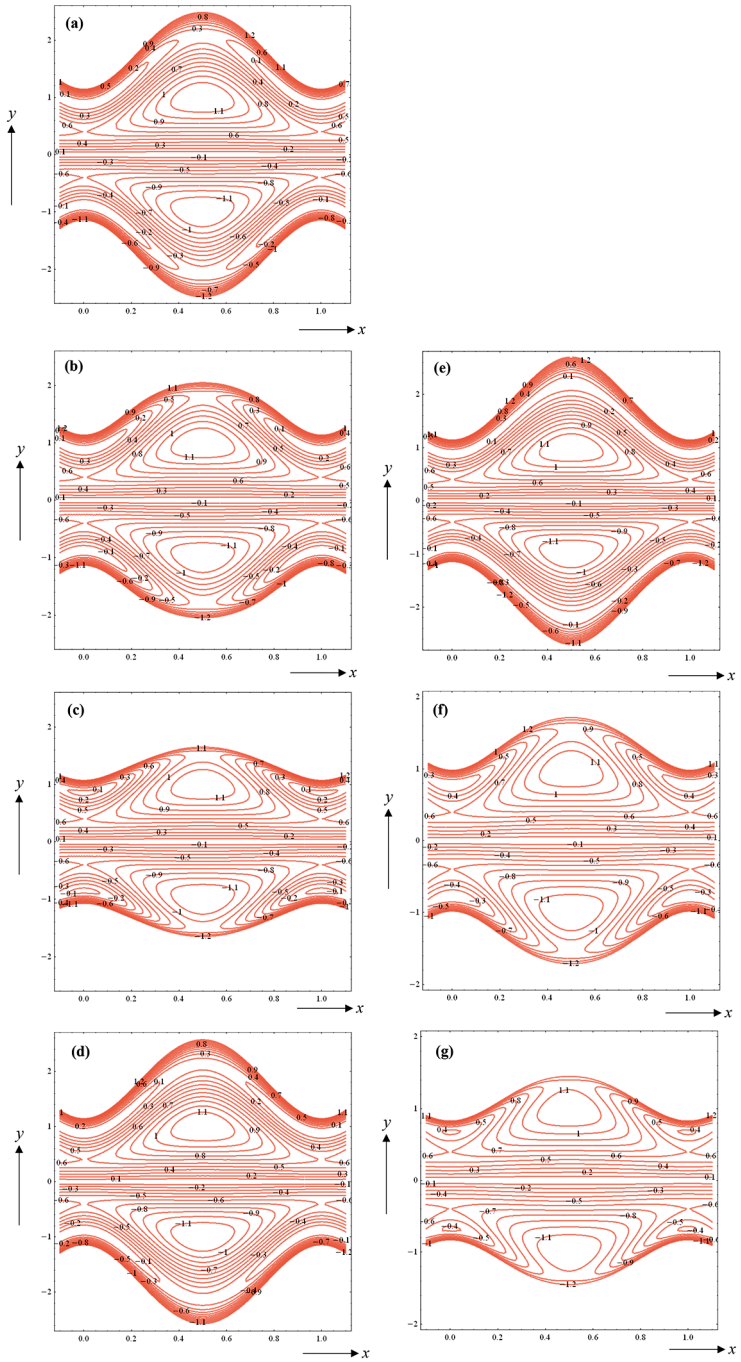

Fig. 6. Stream lines in wave frame at $\phi = 0.6$, $Q = 0.9$ and (a) $\kappa = 2$, $U_{HS} = 1$, $\alpha = 1$, (b) $\kappa = 5$, $U_{HS} = 1$, $\alpha = 1$ (c) $\kappa = 10$, $U_{HS} = 1$, $\alpha = 1$ (d) $\kappa = 2$, $U_{HS} = 0$, $\alpha = 1$ (e) $\kappa = 2$, $U_{HS} = -1$, $\alpha = 1$ (f) $\kappa = 2$, $U_{HS} = 1$, $\alpha = 5$ (g) $\kappa = 2$, $U_{HS} = 1$, $\alpha = 10$.

difference in the conduit. For negative flow rates ($\bar{Q} < 0$), *i.e.* reversed flow, and small values of positive flow rate ($\bar{Q} > 0$), increasing couple stress parameter decreases the pressure difference. In other words, a weaker couple stress rheological effect reduces pressure difference in this range of flow rates. However for larger values of positive flow rate ($\bar{Q} \gg 0$), the opposite effect is induced and there is a growth in pressure difference with increasing couple stress parameter (*i.e.* decreasing couple stress rheological effect).

Figures 5(a)–(c) illustrate the response in local wall shear stress (τ_w) profiles with axial coordinate (x) for different values of the electro-osmotic parameter (κ), maximum electro-osmotic velocity (U_{HS}) and non-Newtonian couple stress parameter (α), respectively. A significant acceleration in the flow and therefore a corresponding increase in wall shear stress magnitudes (note the graph ordinate is plotted so that values decrease upwards along the ordinate) accompanies an increase in the electro-osmotic parameter (κ), as observed in fig. 5(a). Similarly, figs. 5(b) and (c) also demonstrate

that increasing maximum electro-osmotic velocity (U_{HS}) and non-Newtonian couple stress parameter (α), both serve to enhance wall shear stress *i.e.* accelerate the flow at the micro-channel walls. This implies that, respectively, greater axial electrical field and weaker couple stress (micro-structural non-Newtonian behaviour) both boost the momentum in the micro-channel flow and manifest in a significant acceleration at the micro-channel walls. The impact of electrical field (maximum electro-osmotic velocity) is however less prominent than that of couple stress non-Newtonian effect.

Figures 6(a)–(g) visualize the streamline distributions in the channel for various values of electro-osmotic parameter (κ), maximum electro-osmotic velocity (U_{HS}) and non-Newtonian couple stress parameter (α). Comparing fig. 6(a),(b) and (c), for which both U_{HS} and α are given fixed values of unity, and electro-osmotic parameter (κ) varies, it is evident that with greater electro-osmotic effect, the intensity of streamlines near the micro-channel walls is reduced and there is weaker circulation here. A very weak relaxation in the central zone is induced with a slight growth in the dual bolus system present. The streamlines here become more divergent with greater electro-osmotic effect. Comparing fig. 6(d) and (e), for which both κ *and* α are fixed at values of 2 and 1, respectively, and U_{HS} decreases from 0 to -1, it is apparent that with an *decrease* in axial electrical field (to which U_{HS} is proportional) there results an intensification in streamlines near the micro-channel walls although there is no significant modification to the double trapping bolus patterns in the central zone of the channel. The symmetry of the stream function plot is not altered to any great extent; only a very marginal reduction in bolus magnitudes is observed. Finally, inspection of figs. 6(f) and (g), for which both κ *and* U_{HS} are fixed at values of 2 and 1, respectively, and α increases from 5 to 10, a much stronger growth is witnessed in the two trapping boluses and the streamlines become increasingly divergent near the micro-channel walls. Therefore with *weaker actual couple stress rheological effect*, bolus growth is encouraged in the regime. The circulation zones near the micro-channel walls are increasingly less constrained and diverge from each other and there is also greater distortion of the streamlines towards the central zone. The non-Newtonian nature of the fluid therefore imparts a significant influence on bolus dynamics in the micro-channel and leads to a decrease in bolus magnitudes.

4 Conclusions

A theoretical investigation has been conducted for peristaltic propulsion of a couple stress non-Newtonian electro-osmotic electrolyte solution in a micro-channel under the action of a constant strength axial electrical field. The conservation equations for mass, momentum and electrical potential conservation have been linearized using long wavelength, low Reynolds number and Debye-Huckel linearization approximations, the latter invoking the concept of a normalized electro-osmotic potential function. Closed-form solutions for the linearized non-dimensional boundary value problem have been carefully derived for axial velocity, volumetric flow rate, pressure gradient, local wall shear stress and stream function. Numerical evaluation of these expressions with Mathematica software has allowed a parametric study of the influence of electro-osmotic parameter, maximum electro-osmotic velocity and couple stress rheological parameter on the electro-hydrodynamic characteristics of the peristaltic pumping flow. These computations have shown that:

i) Axial pressure gradient ($\frac{\partial p}{\partial x}$) is elevated with increasing electro-osmotic parameter and couple stress parameter (decreasing couple stress rheological effect) and decreased with greater Helmholtz-Smoluchowski velocity.

ii) Axial velocity is consistently enhanced with with increasing electro-osmotic parameter, couple stress parameter (decreasing couple stress rheological effect) and Helmholtz-Smoluchowski (maximum electro-osmotic) velocity.

iii) Pressure differences are consistently enhanced with increasing electro-osmotic parameter and Helmholtz-Smoluchowski (maximum electro-osmotic) velocity both for positive and negative values of the time-averaged volumetric flow rate. However an increase in the couple stress parameter (*i.e.* a decrease in the couple stress rheological effect) only elevates pressure difference for positive values of time-averaged volumetric flow rate, with the contrary effect for negative flow rates.

iv) With greater values of the couple stress parameter, *i.e.*, progressively weaker couple stress non-Newtonian effect, a non-trivial growth is computed in the two trapping boluses and the streamlines become increasingly divergent near the micro-channel walls. Bolus growth is therefore greater for weaker couple stress fluids than stronger couple stress fluids.

v) With weaker assistive axial electrical field (*i.e.* decreasing Helmholtz-Smoluchowski or maximum electro-osmotic velocity) streamlines are intensified near the micro-channel walls although there is no marked alteration in the symmetry or magnitudes of the dual trapped boluses in the central zone of the channel.

vi) With increasing electro-osmotic parameter the intensity of streamlines near the micro-channel walls is reduced (weaker circulation) and furthermore there is a minor growth in the dual trapped boluses present in the core zone of the micro-channel.

References

1. Y. Kang, S.C. Tan, C. Yang, X. Huang, Sens. Actuators A: Phys. **133**, 375 (2007).
2. L. Jiang, J.C. Mikkelsen, J.-M. Koo, D. Huber, S. Yao, L. Zhang, P. Zhou, J.G. Maveety, R. Prasher, J.G. Santiago, T.W. Kenny, K.E. Goodson, IEEE Trans. Compon. Packag., Manufact. Technol. **25**, 347 (2002).
3. Y.K. Suh, S. Kang, *Electroosmotic Pump*, in *Encyclopedia of Microfluidics and Nanofluidics*, edited by D. Li (Springer, US, 2014) pp. 1–13.
4. S. Zeng, C.-H. Chen, J.C. Mikkelsen, J.G. Santiago, Sens. Actuators B **79**, 107 (2001).
5. C.C. Huang, M.Z. Bazant, T. Thorsen, Lab Chip **10**, 80 (2010).
6. S. Liu, Q. Pu, J.J. Lu, J. Chromatogr. A **1013**, 57 (2003).
7. D. Rinderknecht, M.A. Gharib, Acta Futura **6**, 9 (2013).
8. M.A. Benjaminson, S. Lehrer, D.A. Macklin, Acta Astron. **43**, 329 (1998).
9. V.K. Stokes, *Theory of Fluids with Microstructure - An Introduction* (Springer-Verlag, New York, 1984).
10. J. Lin, Comput. Struct. **79**, 801 (2001).
11. M. Nabhani, M. El Khilfi, B. Bou-Said, Tribology Int. **54**, 116 (2013).
12. D. Tripathi, Transp. Porous Media **92**, 559 (2012).
13. D. Pal, N. Rudraiah, R. Devanathan, Bull. Math. Biol. **50**, 329 (1988).
14. D. Tripathi, O. Anwar Bég, J. Mech. Med. Biol. **12**, 1250088 (2012).
15. Y.C. Fung, C.S. Yih, ASME J. Appl. Mech. **35**, 669 (1968).
16. M.Y. Jaffrin, A.H. Shapiro, Annu. Rev. Fluid Mech. **3**, 13 (1971).
17. T.D. Brown, T.K. Hung, J. Fluid Mech. **83**, 249 (1977).
18. Y. Bar-cohen, Z. Chatig, *Piezoelectrically-actuated miniature peristaltic pump*, Caltech-Jet Propulsion Laboratory, Technical Report, Pasadena, California, USA (1991).
19. V. Shkolnikov, J. Ramunas, J.G. Santiago, Sens. Actuators A: Phys. **160**, 141 (2010).
20. E.F. Elsehawey, K.S. Mekheimer, J. Phys. D: Appl. Phys. **27**, 1163 (1994).
21. K.S. Mekheimer, Y. Abdelmaboud, Phys. A: Stat. Mech. Appl. **387**, 2403 (2008).
22. V.P. Rathod, N.G. Sridhar, M. Mahadev, Adv. Appl. Sci. Res. **3**, 2326 (2012).
23. K. Ramesh, M. Devakar, J. Fluids **2015**, 163832 (2015).
24. Y. Abdelmaboud, K.S. Mekheimer, A.I. Abdellateef, ASME J. Heat Transf. **135**, 044502 (2013).
25. D. Tripathi, O. Anwar Bég, Math. Biosci. **246**, 72 (2013).
26. S.-X. Li *et al.*, Colloids Surf. A **470**, 240 (2015).
27. A.A. Siddiqui, A. Lakhtakia, Proc. R. Soc. London A **465**, 501 (2009).
28. A.M. Afonso, M.A. Alves, F.T. Pinho, J. Eng. Math. **71**, 15 (2011).
29. J.J. Sousa, F.T. Pinho, M.A. Alves, Microfluidics Nanofluidics **10**, 107 (2011).
30. G.H. Tang, X.F. Li, Y.L. He, W.Q. Tao, J. Non-Newtonian Fluid Mech. **157**, 133 (2009).
31. G.H. Tang, P.X. Ye, W.Q. Tao, J. Non-Newtonian Fluid Mech. **165**, 1536 (2010).
32. X.X. Li, Z. Yin, Y.J. Jian, L. Chang, J. Su, A.S. Liu, J. Non-Newtonian Fluid Mech. **188**, 43 (2012).
33. M. Rezaei, A.R. Azimian, D. Toghraie, Phys. A: Stat. Mech. Appl. **426**, 25 (2015).
34. G.C. Shit, A. Mondal, A. Sinha, P.K. Kundu, Phys. A: Stat. Mech. Appl. **449**, 437 (2016).
35. G.C. Shit, A. Mondal, A. Sinha, P.K. Kundu, Phys. A: Stat. Mech. Appl. **462**, 1040 (2016).
36. M.F. El-Sayed, M.H. Haroun, D.R. Mostapha, J. Appl. Mech. Tech. Phys. **55**, 565 (2014).
37. P. Goswami, J. Chakraborty, A. Bandopadhyay, S. Chakraborty, Microvascular Res. **103**, 41 (2015).
38. S. Chakraborty, J. Phys. D: Appl. Phys. **39**, 5356 (2006).
39. D. Tripathi, S. Bhushan, O. Anwar Bég, Colloids Surf. A **506**, 32 (2016).
40. N. Rudraiah, B.M. Shankar, C.O. Ng, Spec. Top. Rev. Porous Media **2**, 11 (2011).
41. B.M. Shankar, J. Kumar, I.S. Shivakumara, Appl. Math. Modell. **40**, 5462 (2016).
42. N. Rudraiah, K.S. Mallika, N. Sujatha, J. Appl. Fluid Mech. **9**, 71 (2016).
43. N.S. Akbar, M. Raza, R. Ellahi, Eur. Phys. J. Plus **129**, 155 (2014).
44. N.S. Akbar, S.U. Rahman, R. Ellahi, S. Nadeem, Eur. Phys. J. Plus **129**, 256 (2014).
45. A. Zeeshan, R. Ellahi, M. Hassan, Eur. Phys. J. Plus **129**, 261 (2014).
46. N.S. Akbar, M. Raza, R. Ellahi, Eur. Phys. J. Plus **129**, 185 (2014).
47. R. Ellahi, M.M. Bhatti, I. Pop, Int. J. Numer. Methods Heat Fluid Flow **26**, 1802 (2016).
48. A.C. Eringen, *Microcontinuum Field Theories: II Fluent Media* (Springer, New York, 2001).
49. N.B. Naduvinamani, A. Siddangouda, Proc. IMechE Part J: J. Eng. Tribol. **221**, 525 (2007).
50. S.C. Cowin, Adv. Appl. Mech. **14**, 279 (1974).